Nanoscale

Accepted Manuscript

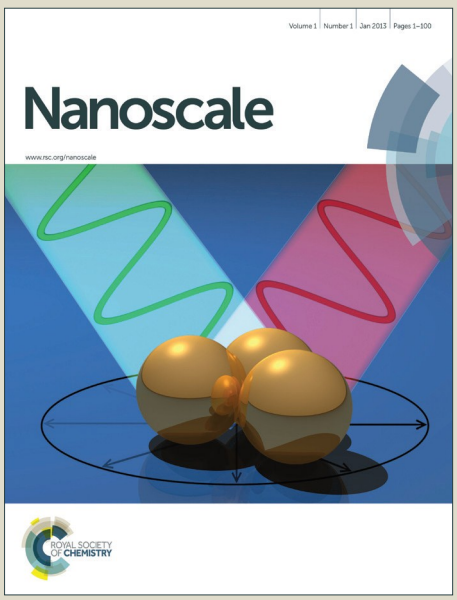

ROYAL SOCIETY OF CHEMISTRY

www.rsc.org/nanoscale

Journal Name

ARTICLE

Multiscale morphology design of hybrid halide perovskite through polymeric template

Received 00th January 20xx,
Accepted 00th January 20xx

DOI: 10.1039/x0xx00000x

www.rsc.org/

Sofia Masi [a,b], Aurora Rizzo [c], Federica Aiello [d], Federica Balzano [d], Gloria Uccello-Barretta [d], Andrea Listorti [b,c], Giuseppe Gigli [c] and Silvia Colella *[a,c]

Hybrid halide perovskites have emerged as promising active constituents of next generation solution processable optoelectronic devices. During their assembling process, perovskite components undergo very complex dynamic equilibria starting in solution and progressing throughout film formation. Finding a methodology to control and affect these equilibria, responsible for the unique morphological diversity observed in perovskite films, constitute a fundamental step towards a reproducible material processability. Here we propose the exploitation of polymer matrices as cooperative assembling components of novel perovskite $CH_3NH_3PbI_3$: polymer composites, in which the control of the chemical interactions in solution allows a predictable tuning of the final film morphology. We reveal that the nature of the interactions between perovskite precursors and polymer functional groups, probed by Nuclear Magnetic Resonance (NMR) spectroscopy and Dynamic Light Scattering (DLS) techniques, allows the control of aggregates in solution whose characteristics are strictly maintained in the solid film, and permits the formation of nanostructures that are inaccessible to conventional perovskite depositions. These results demonstrate how the fundamental chemistry of perovskite precursors in solution has a paramount influence on controlling and monitoring the final morphology of $CH_3NH_3PbI_3$ ($MAPbI_3$) thin films, forseeing the possibility of designing perovskite:polymers composites targeting diverse optoelectronic applications.

Introduction

Hybrid halide perovskites have attracted significant attention due to their outstanding electrical and optical properties.[1-12] Starting from the very first pioneering works,[13-16] a record photoconversion efficiency of 20.1%[17] has been achieved, highlighting the potentiality of these materials as a competitive alternative to thin solid state photovoltaic devices. In addition, perovskites also feature promising light emitting properties, in both optically or electrically driven device configurations.[18-20]

Hybrid perovskites are processable with solution-based techniques at low-temperatures[21-22] and are usually deposited as polycrystalline thin-films with variable mesoscale morphologies, which depend upon growth conditions.[23-26]

The hardly controllable self-assembly process of hybrid perovskite precursors, causing huge morphological variability, results in an intrinsic irreproducibility of the material chemical-physical properties.[27,28] This aspect represents an intrinsic obstacles of $MAPbI_3$ targeting large scale production.

Among the different approaches, such as post-deposition treatments, use of additives etc.,[29-32] a facile method to control the single step growth of methylammonium lead halide perovskite was recently reported. This method proposes the exploitation of macromolecules as templating agents to control the film growth either for solar cells[33-37] or light emitting diodes.[20]

Albeit several efforts have been devoted to the optimization of morphology and processing conditions, very few studies focus on understanding and controlling the chemical interactions occurring in solution, which are instead responsible for the obtainment of optimal film characteristics,[38,39] and consequently are of a paramount importance for optoelectronic device applications. To this purpose, here we present a systematic investigation involving five different polymers: Poly[2-methoxy-5-(2-ethylhexyloxy)-1,4-phenylenevinylene (MEH-PPV), Poly(methylmethacrylate) (PMMA), Poly[(9,9-bis(3'-(N,N-dimethylamino)propyl)-2,7-fluorene)-alt-2,7-(9,9–dioctylfluorene) (PFN), 2,4-Dimethyl-poly(triarylamine (PTAA), Polystyrene (PS) (Figure 1), which

[a] Dipartimento di Matematica e Fisica ''E. De Giorgi'', Universita' del Salento, Via per Arnesano, 73100 Lecce, Italy,
[b] Center for Bio-Molecular Nanotechnology - Fondazione Istituto Italiano di Tecnologia, Via Barsanti, 73010 Arnesano (Lecce), Italy,
[c] CNR-Nanotec - Istituto di Nanotecnologia, Polo di Nanotecnologia c/o Campus Ecotekne, via Monteroni, 73100 Lecce, Italy,
[d] Dipartimento di Chimica e Chimica Industriale, Università di Pisa, Via Moruzzi 13, 561254 Pisa, Italy.
* E-mail: silvia.colella@unisalento.it.

† Electronic Supplementary Information (ESI) available: X-ray diffraction patterns. Absorbance spectra of $MAPbI_3$:polymer mixtures. NMR DOSY maps and ^1H NMR spectra of perovskite and $MAPbI_3$:Polymer blends. This material is available free of charge via the Internet at http://pubs.acs.org. See DOI: 10.1039/x0xx00000x

were selected for the very different electrical and chemical

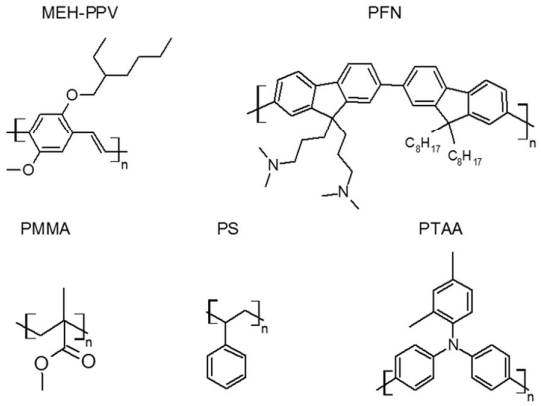

properties with the aim of: *i)* affecting the self-aggregation properties of the perovskite in solution by establishing weak chemical interactions between the perovskite precursors and polymer macromolecules,

Fig.1 Structures of the polymers included in this study.

ii) driving the film growth by acting as three dimensional template for the perovskite aggregates. The final goal is to establish an analytical protocol based on chemical-physical characterization of precursor solutions to predict the resulting material properties in the film. The evolution of polymer-perovskite aggregates from solution to film was followed by a multidisciplinary spectroscopic and microscopic approach. The nature of interactions between polymer and perovskite was probed by using NMR and DLS techniques on the precursor solutions, while Atomic Force Microscopy (AFM) and Scanning Electron Microscopy (SEM) were used to study the distribution of $MAPbI_3$ crystal size in thin solid film. NMR spectroscopy and DLS revealed the presence of a significant self-aggregation of perovskite precursors already in solution strongly affected by the addition of macromolecules, which for their chemical features interfere with the dynamic solvation equilibrium of the ionic species (namely MA^+, PbI_6^{4-}). Notably, we found that MEH-PPV and PFN provide basic functional groups for the establishment of a base-acid equilibrium between the polymer and the MA^+ cation, thus the improved complexing ability evolves in smooth films with uniformly distributed aggregates of tens of nanometers. On the contrary PMMA, PS, PTAA present a much poorer affinity in solution with MA^+ and PbI_6^{4-} ions, leading to severe phase separations during the film forming process and resulting in bigger aggregation of the perovskite domains.

The fine control of the perovskite precursor chemical interactions through the introduction of a macromolecule in solution opens a frontier in the development of new composites where the macromolecule can be specifically designed to achieve the desired chemical and physical properties, according to the kind of application needed. More in general, these findings bring an additional value to the understanding of the perovskite formation chemistry, offering a tool to prevent the aggregation of perovskite by evaluating the efficient solvation of the ionic precursors thus representing a technological advancement towards controlled deposition of these materials.

Experimental

Nanocomposite preparation. The $MAPbI_3$ perovskite was prepared according to the reported procedure.[40] A hydroiodic acid (30 mL, 0.227 mol, 57 wt. % in water, Aldrich) and methylamine (33.7 mL, 0.273 mol, 33% in ethanol, TCI) were stirred under nitrogen atmosphere in the ice bath for 2 h. After stirring at 0° C for 2 h, the resulting solution was evaporated at 50°C for 1 h and produced methylammonium iodide (MAI). Crystallization of MAI was achieved using a rotary evaporator. A white crystalline solid was obtained and washed three times with diethyl ether, dried in a vacuum oven overnight and used without further purification. To prepare $MAPbI_3$ equimolar mixtures of the readily synthesized MAI (0.234 g) and PbI_2 (0.682 g, 99% Aldrich) were mixed in anhydrous dimethylformamide (DMF, 1.5 mL, anhydrous 99.8%, Aldrich) at room temperature. The nanocomposite blends were formed by adding 30 µL of the 40wt% perovskite precursor solution in DMF, to 100 µL of a 5 $mgmL^{-1}$ polymer solution in tetrahydrofuran (THF, anhydrous 99.9%, purchased Aldrich), and by adding dimethyl sulfoxide (DMSO, anhydrous 99.9%, Aldrich) until the final volume of 160 µl. The ratio between polymers and perovskite is 1:36 wt in the final solutions. The solution was shaken in screw-capped glass vials at 25 °C until equilibrium, under nitrogen atmosphere (in glove-box).

Preparation thin film. Thin films were prepared by spin-coating the solutions of polymer filled with perovskite of different concentration at 3,000 rpm for 60 sec, onto the poly(3,4-ethylenedioxythiophene) polystyrene sulfonate (PEDOT:PSS)/glass substrates. The films are annealed at 100 °C for 10 min under nitrogen (glove box).

Materials. For all of our experiments we used:

Poly[2-methoxy-5-(2-ethylhexyloxy)-1,4-phenylenevinylene (MEH-PPV), with weight average molar mass *Mw*=40,000-70,000 $gmoL^{-1}$, purchased from Aldrich Chemical Company;

2,4-Dimethyl-poly(triarylamine (PTAA), with weight average molar mass *Mw*=4,712 $gmoL^{-1}$, purchased from Ossila;

Poly[(9,9-bis(3'-(N,N-dimethylamino)propyl)-2,7-fluorene)-alt-2,7-(9,9–dioctylfluorene) (PFN), with weight average molar mass Mw>10,000$gmLl^{-1}$, purchased from Ossila;

Poly(methyl methacrylate) (PMMA) with weight average molar mass *Mw*=120,000 $gmoL^{-1}$, purchased from Aldrich Chemical Company;

Polystyrene (PS) Mw=70,000 gmL^{-1}, purchased from Aldrich Chemical Company.

Nuclear Magnetic Resonance (NMR) Spectroscopy experiment. Materials. THF-d_8, DMF-d_7 and DMSO-d_6 were purchased from Deutero GmbH (Germany) and employed without further purification.

NMR measurements. ^{1}H NMR measurements were performed on a spectrometer operating at 600 MHz. The temperature was controlled to 25±0.1 °C. The spin-lattice relaxation time (T_1)[41] were measured by using the inversion recovery sequence. Transverse proton relaxation time (T_2)[41] were measured by using the Carr–Purcell–Meiboom–Gill (CPMG) pulse sequence using a pulse spacing of 10 ms for $MAPbI_3$. DOSY (Diffusion Ordered SpectroscopY)[42-44] experiments were carried out by using a stimulated echo sequence with self-compensating gradient schemes and 64K data points. Typically, g was varied in 15 steps (8 transients each) and Δ and δ were optimized in order to obtain an approximately 90-95% decrease in the resonance intensity at the largest gradient amplitude. The baselines of all arrayed spectra were corrected prior to processing the data. After data acquisition, each FID was apodized with 1.0 Hz line broadening and Fourier transformed. The data were processed with the DOSY macro (involving the determination of the resonance heights of all the signals above a pre-established threshold and the fitting of the decay curve for each resonance to a Gaussian function) to obtain pseudo two-dimensional spectra with NMR chemical shifts along one axis and calculated diffusion coefficients along the other. Gradient amplitudes in DOSY experiments have been calibrated by using a standard sample of H_2O 1%.

Preparation of samples. For the first set of measurements NMR samples were prepared according to nanocomposite preparation, i.e. a solution of $MAPbI_3$ in DMF-d_7 (982.76 mM) and a solution 5 $mgmL^{-1}$ in THF-d_8 of each polymer were prepared. Each NMR sample was prepared by adding 131.2 µL of $MAPbI_3$ solution in DMF to 437.6 µL of polymer solution in THF and 131.2 µL of DMSO-d_6 ($MAPbI_3$/polymer 36:1 wt, $MAPbI_3$ 184 mM). After 30 min in vortex (45 °C, 650 rpm) the solutions were transferred into the NMR tube and left to equilibrate before the analysis. For the second set of measurements ($MAPbI_3$/polymer 2:1 wt, $MAPbI_3$ 10 mM) a solution 53.35 mM in DMF-d_7 was used. In the mixture prepared in the presence of PTAA a precipitation occurs, and hence the data were not reported.

Morphological and Structural Analysis of the nanocomposite films. The SEM imaging was performed by the MERLIN Zeiss SEM FEG instrument at an accelerating voltage of 5 kV using an In-lens detector. AFM imaging was carried out in air using a Park Scanning Probe Microscope (PSIA) operating in non-contact mode to reduce tip induced surface degradation and sample damages. The image acquisition was performed in air at room temperature

The XRD spectra of the prepared films were measured with a PAN alytical X'Pert-PRO Materials Research Diffractometer using graphite-monochromated CuKα radiation (λ = 1.5405 Å).

Dynamic Light Scattering (DLS) Measurements. A Zetasizer Nano ZS90 (Malvern, USA) equipped with a 4.0 mW He-Ne laser operating at 633 nm and an Avalanche photodiode detector was used. Measurements were made in low-volume disposable cuvettes kept at 25 °C. Typical concentrations: 1% wt in mixed solvent THF:DMF:DMSO.

Results and discussion

Precursors of $MAPbI_3$, namely methylammonium iodide (MAI) and lead iodide (PbI_2), and their solvation/chemical interaction in solution are the key aspects for determining the characteristics of the resulting solid film. It has recently been demonstrated that perovskite precursor solutions for solar cells are generally colloidal dispersions rather than actual solutions, with colloidal size up to mesoscale.[38] These dispersions are typically stable in polar solvents as DMF or γ-butyrolactone, where solvated ions are in equilibrium till the limit of solubility. The organic component does not only act as reagent for solid phase transformation to perovskite, but also plays a crucial role in coordinating the inorganic component as colloidal soft-framework. Thereby the coordination complex of organic-inorganic components actually determines the final perovskite quality (such as film morphology, grain size, and crystallinity).[27,28] When deposited on the substrate, perovskite materials self-assemble into the crystalline 3D network of PbI_6^{4-} octahedra filled with MA^+ cations. The crystal formation process is relatively rapid (depending on the experimental conditions) and it is difficult to control and to guide its kinetic. The addition of a third component (polymer) in the colloidal dispersion dissolved in a less polar solvent (typically THF) induces the establishment of a different equilibrium involving weak ionic, base-acid, and van der Walls interactions between ions and polymer, inter-ionic interaction and inter-molecular forces between the polymer chains, deeply modifying the coordination chemistry of the original solution. In this complex environment, the physical and chemical properties of the polymer play a crucial role in templating the crystalline growth in a three-dimensional structure and controlling their self-aggregating features in solution and in solid state. We recently reported the successful employment of an amorphous hole-conducting polymer (Poly[2-methoxy-5-(2-ethylhexyloxy)-1,4-phenylenevinylene MEH-PPV)[35] as templating agent for the growth of $MAPbI_3$ perovskite and as active component for photovoltaic applications. We demonstrated that the self-assembly between organic and inorganic moieties is not hindered by the presence of polymer in the precursors solution, which rather improves the film forming capability directly acting on the three dimensional arrangement of the film.

The morphology of a spin-coated polymer-$MAPbI_3$ thin film can be varied *via* the proper selection of the polymer concentration in the polymer-$MAPbI_3$ solution, the use of different spin speeds/spin time, as well as the different drying rates of the solvent, in order to accommodate requirements for different applications. In our case of study, we keep all the parameters constant but the chosen polymer, that will be, therefore, the only responsible for the changes in the film.

Distinct self-assembly environments are created in solution when different polymers interact with perovskite precursors, leading to different types of electrostatic interactions between the positively charged precursor MA^+, and the counter-anion, PbI_6^{4-}. Non-covalent interactions including π–π stacking, hydrophobic interactions, and hydrogen-bonding are key elements for the self-assembly.

With the aim of detecting interaction phenomena involving $MAPbI_3$ and polymeric materials, namely MEH-PPV, PMMA, PFN, PS (Figure 1), we carried out a Nuclear Magnetic Resonance (NMR) spectroscopy investigation in solution. Among the NMR parameters, we focused on diffusion coefficients (D, m^2s^{-1}), longitudinal relaxation times T_1 (s) and transverse relaxation times T_2 (s), which are expected to be responsive to aggregation phenomena. We compared NMR parameters (P) of the methyl

protons of pure $MAPbI_3$ and its mixtures with the polymers. An interaction of $MAPbI_3$ with polymeric materials is expected to bring about a decrease both of diffusion coefficients and relaxation times. The preliminary comparison of ^1H NMR spectra of $MAPbI_3$ and its mixtures with selected polymers revealed that fast exchange conditions hold, being observed only one signal for $MAPbI_3$ in its free and bound states. In these conditions, the measured NMR parameter (P_{obs}) represents the weighted averaged of its value in the free (P_f) and bound (P_b) states as in the equation 1

$$P_{obs} = x_b P_b + x_f P_f \quad \text{(eq. 1)}$$

where x_f and x_b are the molar fractions in free and bound state, respectively.

Firstly, NMR experiments were performed on the pure $MAPbI_3$ solutions, investigating the effect of different concentrations spanning from the one used for the preparation of the blends (184 mM) till much lower content. We found that the diffusion coefficient was sensitive to concentration gradients, since the value of $9.9 \times 10^{-10} m^2 s^{-1}$ was measured at 184 mM, which increased till to $10.4 \times 10^{-10} m^2 s^{-1}$ at 10 mM and $12.7 \times 10^{-10} m^2 s^{-1}$ at 2 mM (Supporting Information Figure S1). This result is in keeping with the propensity of $MAPbI_3$ to self-aggregate, as also reported in previous works.[38]

The optimal experimental conditions for NMR measurements (further details are reported in Supporting Information) involved analyses of mixtures where $MAPbI_3$ was kept constant at 10 mM (6.20 $mgmL^{-1}$) in the presence of 3.13 $mgmL^{-1}$ polymer.

For PTAA, reproducible results could not be obtained due to the much lower solubility in the solvent mixture.

Diffusion coefficients did not show significant changes as the consequence of the presence of polymeric materials, probably due to the competition between self-aggregation and $MAPbI_3$/polymer interactions. By contrast, transverse relaxation times T_2 underwent significant changes (Table 1) in particular in the presence of MEH-PPV: its value decreased from 2.50 ± 0.05 s to 0.63 ± 0.05 s, thus suggesting a strong interaction between $MAPbI_3$ and the polymer. Longitudinal relaxation parameters (T_1) also underwent a sensitive change from 3.27 ± 0.05 s to 2.82 ± 0.05 s (Table 1). No relevant changes were detected in the presence of the other polymers.

Due to the much lower number of repeating units in PFN, in order to obtain comparable data with respect to MEH-PPV in terms of similar ratio between $MAPbI_3$ and repeating unit of the polymer (reported in Table 1), we increased the PFN concentration until 8.61 $mgmL^{-1}$ (0.83:1 $MAPbI_3$/repeating unit of polymer, as reported in Table 2). This caused a sensitive decrease of T_2 of $MAPbI_3$ also in the presence of PFN (1.66 ± 0.05 s instead of 2.36 ± 0.05 s). Therefore, it can be reliably assessed that, among analysed polymers, MEH-PPV and PFN both originate remarkable intermolecular interactions with $MAPbI_3$, but complexation phenomena are more favourite in $MAPbI_3$/MEH-PPV blends. For the two higher *Mw* polymers (PMMA and PS), which did not perturb T_2 of $MAPbI_3$, a lower ratio between $MAPbI_3$ and repeating units of polymer is present, therefore the univocal interpretation of data did not require changes of polymers amounts. It is noteworthy that a further addition of MEH-PPV (12.14 $mgmL^{-1}$) in the NMR tube brought about the expected decrease of relaxation parameters of $MAPbI_3$ (2.40 ± 0.05 s for T_1 and 0.55 ± 0.05 s for T_2). In order to minimize the self-aggregation of $MAPbI_3$, a further set of measurements was performed, where $MAPbI_3$ concentration was lowered to 2 mM (1.24 $mgmL^{-1}$). Unfortunately, a superimposition of signals of $MAPbI_3$ and DMSO was observed in the mixtures containing the polymers (Supporting Information Figure S2). After a screening of solvent mixtures, we find a good separation of these two signals by employing THF/DMSO 5:2 as solvent mixture. After a screening of solvent mixtures, we find a good separation of these two signals by employing THF/DMSO 5:2 as solvent mixture.

Interestingly, in these experimental conditions also the diffusion coefficient of $MAPbI_3$ became sensitive to the presence of MEH-PPV.

Its value decreased from $13.5 \times 10^{-10} m^2 s^{-1}$ for the pure compound until $11.9 \times 10^{-10} m^2 s^{-1}$ in the mixture (molar ratio P3/MEH-PPV 0.83:1, Figure S3).

Table 1- Average number of polymer units, spin lattice relaxation time (T_1, s) and spin-spin relaxation time (T_2, s) of $MAPbI_3$ (P3) (6.20 $mgmL^{-1}$) free and in the presence of polymers (3.13 $mgmL^{-1}$).

	P3	P3/PMMA	P3/MEH-PPV	P3/PFN	P3/PS
Polymer units		1,198	211	14	673
$MAPbI_3$/ polymer units		0.32:1	0.83:1	2.29:1	0.33:1
T_1*	3.27	3.31	2.82	3.27	3.34
T_2*	2.50	2.60	0.63	2.36	2.64
*Error on T_1 and T_2 is ± 0.05.					

Table 2- spin lattice relaxation time (T_1, s) and spin-spin relaxation time (T_2, s) of $MAPbI_3$ (P3) (6.20 $mgmL^{-1}$) free and in the presence of polymers (8.6 $mgmL^{-1}$ for PFN and 3.13 mgm L^{-1} for MEH-PPV).

	P3	P3/MEH-PPV	P3/PFN
$MAPbI_3$/polymer units		0.83:1	0.83:1
T_1*	3.27	2.82	3.20
T_2*	2.50	0.63	1.66
*Error on T_1 and T_2 is ± 0.05.			

With the aim of further exploring the interactions between polymers and perovskite precursors and assessing the colloidal tunability in more detail by the polymer choice, DLS was employed to verify the size distribution of dispersion in the precursor solutions. By DLS we could estimate the presence of aggregates, both in the isolated $MAPbI_3$ and polymers solutions, and in the $MAPbI_3$:polymer blends. In particular, we focused on observing the behaviour of polymer solutions before and after the addition of perovskite precursors.

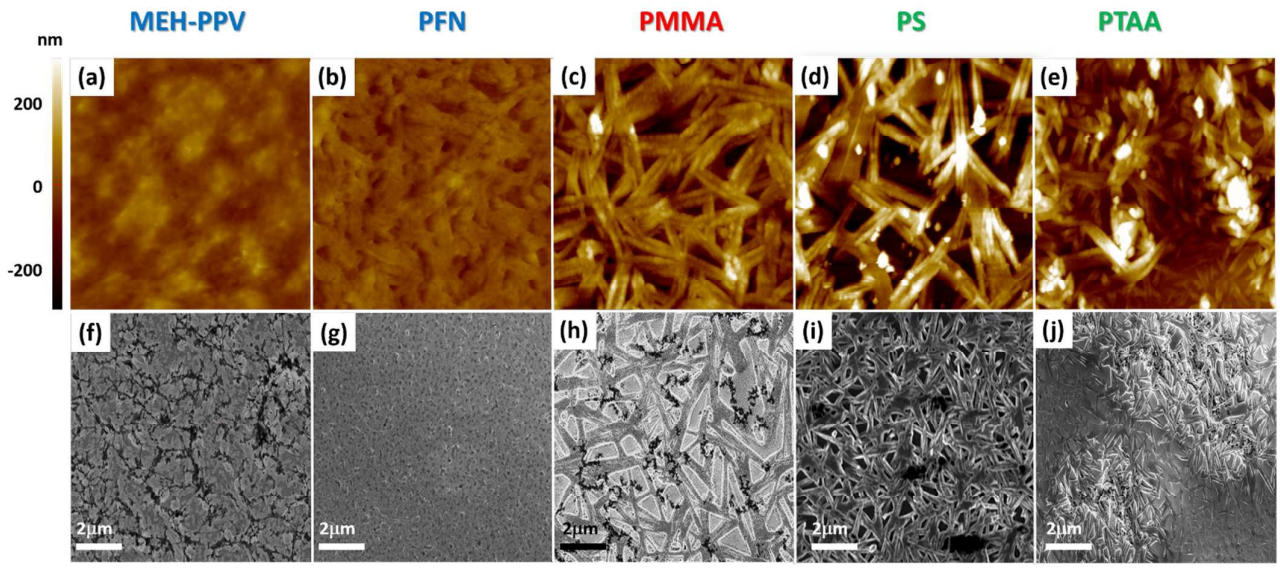

Figure 2. Dynamic light scattering profiles of a.) $MAPbI_3$ formulation in DMF:THF:DMSO and after conjugation to polymers b.) MEH-PPV, c.) PFN, d.)PMMA, e.)PS, f.)PTAA.

Fig 3. AFM images of polymer:$MAPbI_3$ (a-e). The scale bar is 20 (µm) x 20 (µm.) SEM images of polymer:$MAPbI_3$ (f-j). The scale bar is 2 µm.

In Figure 2, reporting the statistical distribution of the measured hydrodynamic diameter (D_h), we can observe a first clear difference among the free polymer solutions due to the relative solubility in the employed mixture of solvents.

The size of aggregates, spanning from 8 nm to 50 nm, reveals in average a good solubility for PFN (D_h= 8 nm, 28 nm), PMMA (D_h= 40 nm), PS (D_h= 30 nm) and MEH-PVV (D_h= 50 nm). MEH-PPV presents a second statistical population of much larger aggregates (500 nm) due to its tendency to form a gel-like solution, while PTAA, due to its low solubility in the employed solvents, shows uniformly distributed large aggregates in solution (D_h= 600 nm). Despite PMMA and PS showed relatively small aggregates in solution, in the presence of perovskite precursors we could observe a significant shift of the signal indicating much larger aggregates size (D_h= 250 nm and 500 nm respectively) than bare perovskite precursors (160 nm) and polymer (40 and 30 nm) solutions.

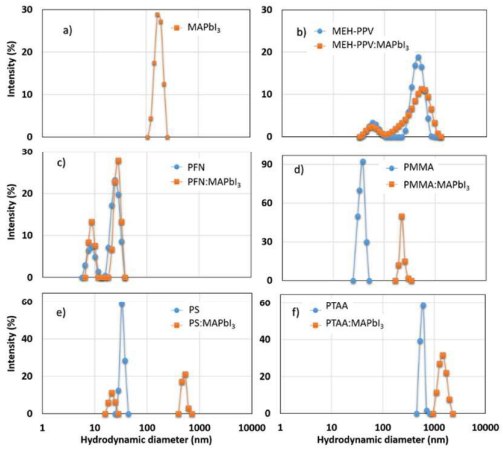

For MEH-PPV and PFN, instead, aggregate size maintained the same statistical distribution following the addition of perovskite precursors. Last, for PTAA we registered a shift in the presence of perovskite ions from D_h= 600 nm to D_h= 1500 nm (Figure 2). Due to the similarity of the peak size and distribution for the mixed samples $MAPbI_3$:PFN, $MAPbI_3$:MEH-PPV and the corresponding bare polymer solutions, we hypothesize that a high degree of association occurs between the polymer and perovskite components. Such a behaviour could be induced by the interactions between the very basic trialkylammonium groups in the side chain of PFN and ether groups of MEH-PPV with perovskite precursors. Those results are in line with the trend found by NMR. On the contrary, it was found that PTAA, PMMA and PS formulations present bigger aggregates following the addition of PbI_2 and MAI in solution, likely due to a phase separation and aggregation of polymer itself.

Following the studies in solution, in order to elucidate the effect of the different polymers on the self-assembly process, we investigated the morphological features of the deposited polycrystalline films in various macromolecule environment; the solutions were spin-coated on the substrates, and the resulting polymer:perovskite blends examined by AFM and SEM (Figure 3). First, we ensure the formation of the desired perovskite structure by the collection of X-ray diffraction patterns and absorption spectra, reported in Figure S4 and S5, respectively. XRD patterns (Figure S4) revealed a $MAPbI_3$ perovskite tetragonal phase showing no preferential

orientation of the crystalline domains.[45,46] The main diffraction peaks, assigned to the (110), (220), (312) and (224) faces, are common and found at identical angles, namely 14.05°, 28.38°, 31.74° and 40.63° for all the blends, confirming the formation of perovskite crystals with the same tetragonal structure independently on the polymer matrix.

Furthermore we monitored the time-course increase of the PbI_2 characteristic peak (12.6°) intensity for the studied films exposed to ambient conditions, in order to evaluate the decomposition kinetics of $MAPbI_3$ with and without polymer template. We verified an improved stability to moisture for all of the composites with respect to the pristine $MAPbI_3$ film, as shown in Figure S4, possibly due to a preferential location of the macromolecules at the perovskite polycrystals grain boundaries, which are typically the ones more unstable and subject to attack by moisture. [47]

All the samples, except for the PTAA, have comparable absorption (Figure S5). The lower absorption for PTAA is likely due to the formation of very big and not uniform perovskite aggregates in the composite film.

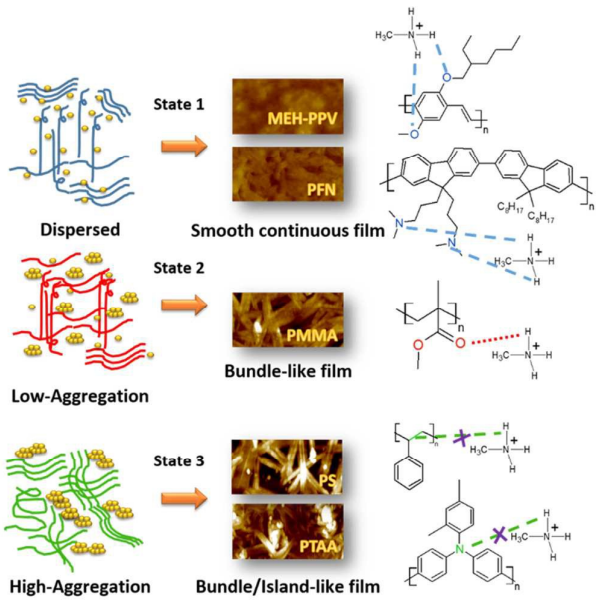

Scheme 1. Simplified illustration of the studied nanocomposites grouped in 3 different states according with the diverse morphologies obtained and related to the degree of chemical affinity between polymer and MA^+.

Topography images collected for the polymer:perovskite films clearly showed the contribution of basic functional groups in the formation of smooth film (root mean square roughness Rq = 27nm for MEH-PPV and Rq= 33 nm for PFN, from AFM).

As shown in SEM images (Figure 3), we consistently observe perovskite aggregates having a relatively uniform width of ~40-50 nm and similar shape for $MAPbI_3$:MEH-PPV and ~10-20 nm for $MAPbI_3$:PFN systems. Accordingly to the previous observation about the affinity between perovskite and MEH-PPV functional groups, $MAPbI_3$:MEH-PPV film results homogeneous due to the smallest perovskite aggregate. Furthermore, MEH-PPV, due to its lower solubility in the solvent mixture with respect to PFN and its tendency to form a very viscous solution, gives rise to amorphous polymer rich domains alternating the perovskite domains, as clearly shown by SEM picture, which contribute to the smoothness of the film. At support of this point, AFM images on the polymer:perovskite films evidenced the contribution of basic functional groups in the formation of smooth film with roughness values of Rq = 27 nm for MEH-PPV and Rq= 33 nm for PFN, while rougher films are obtained for PMMA= 135 nm, for PS = 197 nm and for PTAA = 202 nm. On the other hand, a bundle-like crystal structure characterizes the PS, PMMA and PTAA blends, differing for the aggregates dimension and roughness, which vary coherently with the aggregate size found from DLS analysis and with the poor interaction we found by NMR. Films prepared from the $MAPbI_3$: PMMA, $MAPbI_3$: PS and $MAPbI_3$:PTAA blends showed very large size aggregates (100-150 nm), leading to a multi-scale roughness (Rq>100 nm) and not uniform surface coverage because of the unfavourable polymeric environment, which impedes an ordered growth of the crystalline perovskite phase. In particular, PS and PTAA:$MAPbI_3$ nanocomposites represent the extreme cases, due to the strongly apolar nature of the polymers, resulting in a quite non-uniform film where polymer and perovskite grow in two completely separated phases. Along with the bundle-like morphology, we can gather the presence of micron-size aggregates (see Figure 3d-e). Overall the polymer:perovskite nanocomposites have very different morphology from the pristine $MAPbI_3$ film (see Figure S6), further evidencing the active role of the polymer in guiding the perovskite growth.

Scheme 1 shows the summary of the different situations we encountered for the perovskite precursors aggregation features in combination with the polymer matrices in solution, thus to their tendency to transfer the aggregates to the solid film, depending on the degree of intermixing between the macromolecules and the ions.

As illustrated with simplified schemes, State 1 represents a situation where there is a good chemical affinity between the ions in solution and the polymer functional groups, in which we identify the case of MEH-PPV and PFN blends with $MAPbI_3$ resulting in a smooth surface where perovskite precursors aggregates in small and uniformly distributed domains. The polymer matrix, thanks to hydrogen bonds with MA^+ cation, likely guide the formation of perovskite crystal during the self-assembly process, to finally locate at the grain boundaries between perovskite polycrystals, due to its amorphous nature. As the basic character decreases from ethereal to ester moieties, presenting pKa respectively of -6.5 and -3.5,[48] the tendency to give hydrogen bonds also decreases, thus perovskite precursors tend to aggregate, as represented by the state 2, in which we collocate PMMA. More severe particle aggregation is induced by PS and PTAA (state 3), due to their apolar nature, leading to bundle/island-like morphology after coating and drying, which is referred to as the high aggregation state.

Conclusions

We conclude that the use of polymers as cooperative additives for hybrid halide perovskite growth enhances the morphology control over the polycrystalline film formation. We highlight how the self-aggregation properties and the complex dynamic equilibria existing in solution between the perovskite precursors are profoundly modified by the chemical interaction with the macromolecule and, most importantly, can be directly transduced into the morphological features of the solid thin film.

We investigate the influence of the strength of non-covalent polymer–perovskite interactions between MA^+ precursor and functional groups by means of NMR spectroscopy, while the tendency of the various components to aggregates are studied by DLS.

Hydrogen bonds are found responsible for the association of MA^+ cation and polymers. The MA^+ acid hydrogen atom form a link with oxygen atom electron pairs belonging to ethereal functional groups of MEH-PPV and of nitrogen atoms of pending groups of PFN, as detected by T_2 spin relaxation time measurements. Reduced basic character of ester moieties of PMMA and steric hindrance in tri-phenyl substituted nitrogen of PTAA as well as the absence of hydrogen-bonds donor/acceptor groups in PS lead to a remarkably reduced of these polymers interaction with MA^+. The solution measurements of relaxation parameters of MA^+ in the presence of polymeric materials could become a suitable probe for controlling perovskite morphologies, in consideration of the fact that predictably smother morphologies, characterized by more interconnected domains, are associated to higher decrease of relaxation parameters. Furthermore we prove that the deposition of the perovskite in the presence of polymers exhibit increased moisture stability as compared to bare perovskite. These findings contribute to shine light on the complex coordination chemistry of hybrid halide perovskite and on its correlation with the polycrystalline film morphology. Moving from these observation would be possible to target alternative polymers or single molecules with specific functional groups capable of differently interact with perovskite constituents aiming at mastering the solution equilibria of those to the final film formation.

Acknowledgements

SM, SC, AL, AR and GG acknowledge Progetto di ricerca PON R&C 2007-2013 (Avviso n. 713/Ric. del 29 ottobre 2010) MAAT-Molecular NAnotechnology for HeAlth and EnvironmenT (Project Number: PON02_00563_3316357), EFOR-Energia da FOntiRinnovabili (Iniziativa CNR per il Mezzogiorno L. 191/2009 art. 2 comma 44), Regione PUGLIA (APQ Reti di Laboratorio, project "PHOEBUS" cod. 31), SC and GG acknowledge the project Beyond-Nano (Project Number: PON03_00362) for financial support. AR gratefully acknowledge SIR Two-Dimensional Colloidal Metal Dichalcogenides based Energy-Conversion Photovoltaics (2D ECO), Bando SIR MIUR Decreto Direttoriale 23 gennaio 2014 n. 197, Project Number: RBSI14FYVD. The authors gratefully acknowledge Sonia Carallo for technical support.

References

1 H.S. Jung and N.G. Park, *Small,* 2015, **11**, 10-25.

2 M. A. Green, A. Ho-Baillie, H. J. Snaith, *Nat Photonics,* 2014, **8**, 506-514.

3 P. Gao, M. Gratzel, M. K. Nazeeruddin, *Energy Environ. Sci.,* 2014, **7**, 2448-2463.

4 S. Shi, Y. Li, X. Li, Wang, H. *Materials Horizons,* 2015, DOI: 10.1039/c4mh00236a.

5 F. Deschler, M. Price, S. Pathak, L. E. Klintberg, D.D. Jarausch, R. Higler, S. Huttner, T. Leijtens, D. S. Stranks, H. J. Snaith, M. Atature, R. T. Phillips, R.H. Friend, *.J. Phys. Chem. Lett.,* 2014, **5**, 1421-1426.

6 C. Wehrenfennig, M. Liu, H. J. Snaith, M. B. Johnston, L. M. Herz, *J. Phys. Chem. Lett.,* 2014, **5**, 1300-1306.

7 G. Xing, N. Mathews, S. S. Lim, N. Yantara, X. Liu, D. Sabba, M. Gratzel, S. Mhaisalkar, T. C. Sum, *Nat Mater,* 2014, **13**, 476-480.

8 Z. K.Tan, R. S. Moghaddam, M. L. Lai, P. Docampo, R. Higler, F. Deschler, M. Price, A. Sadhanala, L. M. Pazos, D. Credgington, F. Hanusch, T. Bein, H. J. Snaith, R. H. Friend, *Nat Nanotechnol.,* 2014, **9**, 687-692.

9 A. Sadhanala, A. Kumar, S. Pathak, A. Rao, U. Steiner, N. C. Greenham, H. J. Snaith, R. H. Friend, *Adv. Electron. Mater.,* 2015, **1**, 3, DOI: 10.1002/aelm.201500008.

10 H. J. Snaith, *J. Phys. Chem. Lett.,* 2013, **4**, 3623-3630.

11 Q. Dong, Y. Fang, Y. Shao, P. Mulligan, J. Qiu, L. Cao, H. Jinsong, *Science,* 2015, **347**, 967-970.

12 M. A. Green, A. Ho-Baillie, H. J. Snaith, *Nat. Photonics,* 2014, **8**, 506-514.

13 A.Kojima, K. Teshima, Y. Shiray, T. Miyasaka, *J. Am. Chem. Soc.*, 2009, **17** (131), 6050–6051

14 J-H. Im, C-R. Lee, J-W. Lee, S-W. Park, N-G. Park, *Nanoscale*, 2011, **3**, 4088-4093

15 H-S. Kim, C-R. Lee, J-H Im, K-B. Lee, T. Moehl, A. Marchioro, S-J. Moon, R. Humphry-Baker, J-H. Yum, J. E. Moser, M. Gratzel, N-G. Park, Sci Rep. 2012, **2**, 591.

16 M. M. Lee, J. Teuscher, T. Miyasaka, T. N. Murakami, H. J. Snaith, *Science,* 2012, **338**, 643.

17 W. Yang, J. H. Noh, N. J. Jeon, Y. C. Kim, S. Ryu, J. Seo, S. I. Seok, *Science express*, 2015, 10.1126/science.aaa9272.

18 R. L. Z. Hoye, M. R. Chua, K. P. Musselman, G. Li, M. L. Lai, Z. K. Tan, N. C. Greenham, J. L. McManus-Driscoll, R. H. Friend, D. Credgington, *Adv. Mater.,* 2015, **27**, 1414-1419.

19 J. Wang, N. Wang, Y. Jin, Y. Si, Z. K. Tan, H. Du, L. Cheng, *X.* Dai, S. Bai, H. He, Z. Ye, M. L. Lai, R. H. Friend, W. Huang, *Adv. Mater.,* 2015, **27**, 2311-2316.

20 G. Li, Z. K. Tan, D. Di, M. L. Lai, L. Jiang, J. H.-W. Lim, R. H. Friend, N. C. Greenham, *Nano Letters,* 2015, **15**(4), 2640–2644.

21 J. Burschka, N. Pellet, S. J. Moon, R. Humphry-Baker, P. Gao, M. K. Nazeeruddin, M. Gratzel, *Nature*, 2013, **499**, 316 – 319.

22 S. Ryu, J. H. Noh,N. J. Jeon, Y. Chan Kim, W. S. Yang, J. Seo, S. I. Seok, *Energy Environ. Sci.,* 2014, **7**, 2614–2618.

23 V. L. P. Guerra, D. Altamura, V. Trifiletti, S. Colella, A. Listorti, R. Giannuzzi, G. Pellegrino, G.G. Condorelli, C. Giannini, G. Gigli, A. Rizzo, *J. Mat. Chem. A*, 2015, DOI: 10.1039/C5TA05220C.

24 G. Pellegrino, S. Colella, I. Deretzis, G. G. Condorelli, E. Smecca, G. Gigli, A. La Magna, A. Alberti, *J. Phys. Chem. C*, 2015, **119** (34), 19808–19816.

25 V. Trifiletti, V. Roiati, S. Colella, R. Giannuzzi, L. De Marco, A. Rizzo, M. Manca, A. Listorti, G. Gigli, *ACS Appl. Mater. Interfaces*, 2015, ***7*** (7), 4283–4289.

26 A. Listorti, E. J. Juarez-Perez, C. Frontera, V. Roiati, L. Garcia-Andrade, S. Colella, A. Rizzo, P. Ortiz, I. Mora-Sero, *J. Phys. Chem. Lett.*, 2015, ***6*** (9), 1628–1637.

27 J.-H. Im, I.-H. Jang, N. Pellet, M. Grätzel, N. G. Park, N*at.Nanotechnol.* 2014, **9**(11), 927-32.

28 M. De Bastiani, V. D'Innocenzo, S. D. Stranks, H. J. Snaith, A. Petrozza, *APL Mater.* 2014, **2**, 081509.

29 W. Nie, H. Tsai, R. Asadpour, J. C. Blancon, A. J. Neukirch, G. Gupta, J. J. Crochet, M. Chhowalla, S. Tretiak, M. A. Alam, H. L. Wang, A. D. Mohite, *Science,* 2015, **347**, 522-525.

30 S. D. Stranks, G. E. Eperon, G. Giulia, M. Christopher, M. J. P. Alocer, T. Leijtens, L. M. Herz, A. Petrozza, H. J. Snaith, *Science*, 2013, **342**, 341–344.

31 G. Xing, N. Mathew, S. Sun, S. S. Lim, Y. M. Lam, M. Gratzel, S. Mhaisalkar, T. C. Sum, *Science*, 2013, **342**, 344–347.

32 C. Wehrenfennig, G. E. Eperon, M. B. Johnston, H. J. Snaith, L. M. Herz, *Adv. Mater*. 2014, **26**, 1584–1589.

33 Z. Cheng, J. Lin, *CrystEngComm*, 2005, **12**, 2646-2662.

34 S. F. Luan, Z. Y. Cheng, R. B. Xing, Z. Wang, X. H. Yu and Y. C. Han, *J. Appl. Phys.*, 2005, **97**, 086102.

35 S. Masi, S. Colella, A. Listorti, V. Roiati, A. Liscio, V. Palermo, A. Rizzo, G. Gigli, *Sci. Rep*. 2015, **5**, 7725.

36 Q. Xue, Z. Hu, C. Sun, Z. Chen, F. Huang, H. L. Yip, Y. Cao; *RSC Adv*., 2015, **5**, 775–783.

37 C. Y. Chang, C. Y. Chu, Y. C. Huang, C. W. Huang, S. Y. Chang, C. A. Chen, C. Y. Chao, F. W. Su, *ACS Appl. Mater. Intefaces*, 2015, ***7*** (8), 4955–4961.

37 T. Ding, X. Yao, C. Wei, Y. Zhao, *J. power sources*, 2014, **272**, 351-355.

38 K. Yan, M. Long, T. Zhang, Z. Wei, H. Chen, S. Yang, I. Xu, *J. Am. Chem. Soc.*, 2015, **137** (13), 4460–4468.

39 S. T. Williams, F. Zuo, C-C. Chueh, C. Y. Liao, P. W. Liang, A. K.Y. Jen, *ACS Nano*, 2014, **8** (10), 10640-10654.

40 M. M. Lee, J. Teuscher,T. Miyasaka, T. N. Murakami, H. J. Snaith, *Science*, 2012, 338, 643–647.

41 D. Neuhaus, M. Williamson, *The nuclear Overhauser effect in structural and conformational analysis*; VCH: New York, 1989; 8-13.

42 A. Macchioni, G. Ciancaleoni, C. Zuccaccia, D. Zuccaccia, P. A. Gale, J. W. Steed, *Supramolecular Chemistry: From Molecules to* Nanomaterials; Gale, P.; Steed, J., Eds.; Wiley and Sons: Chichester, U.K., 2012; Vol. **2**, pp. 319-330.

43 G. A. Morris, *Multidimensional NMR Methods for the Solution State*; G. A. Morris, J. W. Emsley, Eds.; Wiley and Sons: Chichester, U.K., 2010; pp. 515-532.

44 G. A. Morris, *Encyclopedia of Nuclear Magnetic Resonance*; Grant, D. M., Harris, R. K., Eds.; Wiley and Sons: Chichester, U.K., 2002; Vol. **9**, pp. 35–44.

45 N. J. Jeon, J. H. Noh, Y. C. Kim, W. S. Yang, S. Ryu, S. I. Seok, *Nat. Mater.*, 2014, **13**, 897–903.

46 S. Colella, E. Mosconi, P. Fedeli, A. Listorti, F. Gazza, F. Orlandi, P. Ferro, T. Besagni, A. Rizzo, G., F. De Angelis, R. Mosca, *Chem. Mater.*, 2013, **25**, 4613–4618.

47 Q. Chen, H. Zhou, T-B. Song, S. Luo, Z. Hong, H-S Duan, L. Dou, Y. Liu, Y. Yang, Nano Lett., 2014, **14**, 4158–4163.

48 N. L. Allinger, M. P. Cava, D. C. D. Jongh , C. R. Johnson , N. A. Lebel , C. L. Stevens, *CHIMICA ORGANICA*, ed Zanichelli 1981, pp. 252.